ACS APPLIED MATERIALS & INTERFACES

Research Article

www.acsami.org

Control of the Particle Distribution in Inkjet Printing through an Evaporation-Driven Sol–Gel Transition

Emma L. Talbot,[†] Lisong Yang,[†] Arganthaël Berson,[‡] and Colin D. Bain*[,†]

[†]Department of Chemistry, Durham University, Durham DH1 3LE, United Kingdom

[‡]School of Engineering and Computing Sciences, Durham University, Durham DH1 3LE, United Kingdom

Supporting Information

ABSTRACT: A ring stain is often an undesirable consequence of droplet drying. Particles inside evaporating droplets with a pinned contact line are transported toward the periphery by radial flow. In this paper, we demonstrate how suspensions of laponite can be used to control the radial flow inside picoliter droplets and produce uniform deposits. The improvement in homogeneity arises from a sol–gel transition during evaporation. Droplets gel from the contact line inward, reducing the radial motion of particles and thus inhibiting the formation of a ring stain. The internal flows and propagation of the gelling front were followed by high-speed imaging of tracer particles during evaporation of the picoliter droplets of water. In the inkjet nozzle, the laponite network is broken down under high shear. Recovery of the low shear viscosity of laponite suspensions was shown to be fast with respect to the lifetime of the droplet, which was instrumental in controlling the deposit morphology. The radial and vertical particle distributions within dried deposits were measured for water droplets loaded with 1 and 5 wt % polystyrene spheres and various concentrations of laponite. Aggregation of the polystyrene spheres was suppressed by the addition of colloidal silica. The formulation can be tuned to vary the deposit profile from a ring to a pancake or a dome.

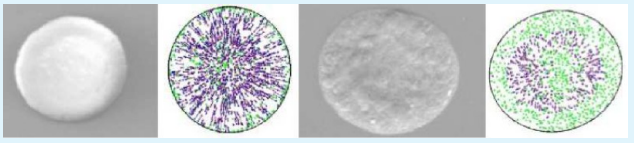

KEYWORDS: *coffee ring, droplet deposition, inkjet printing, profile control, laponite additive, sol–gel transition*

INTRODUCTION

Inkjet printing is a widely used noncontact method for delivering colloidal suspensions onto substrates.[1] A uniform particle distribution in the deposit is usually desired. For example, in graphical printing, a uniform deposit requires the minimum amount of ink for a given color density. A contact line that is pinned at a constant radius is also desirable to produce a well-defined edge to the deposit: contact lines that retract during drying often lead to irregular deposits and poorly controlled properties. Pinning is common on rough[2,3] or chemically inhomogeneous substrates[4,5] and for fluids containing high solid loadings.[6−8]

While a uniform particle distribution is the ideal, often a ring stain is the reality.[9−13] For a sessile droplet with a contact angle of less than 90°, evaporation is greatest at the contact line. If the contact line is pinned, fluid flows toward the periphery, replenishing liquid lost due to evaporation.[14] Particles inside the droplet are transported to the contact line and build up a ring stain (the "coffee ring effect").[9] Particle migration within drying droplets can also produce a nonuniform deposit.[15,16] A nonuniform particle distribution reduces the quality of graphical printing because the optical density varies across the deposit. Similarly, printed electronics are limited by variation of the conductivity or porosity across a printed feature.[17−19] Biological assays based on inkjet technology also need a uniform concentration of material across the deposit to be most effective.[20]

A number of methods have been proposed to suppress ring stains. Mechanical methods such as selective laser sintering[21] or multiple passes of the print-head adjust the profile of the end deposit through the physical addition or removal of material. Schirmer et al. filled in the ring stains using multiple droplets, each forming a smaller concentric ring stain.[22]

Other methods exploit the underlying solvent properties or include additives to alter the flow pattern. Reducing the radial flow, or changing the flow pattern from radial to circulating, inhibits the formation of a ring stain by limiting the supply of colloidal material to the contact line. Radial flow has been reduced or prevented by adjustment of the solvent composition in the ink,[13,23−26] by control of the substrate temperature,[27,28] or by a combination of flow manipulation and contact line depinning using electrowetting.[29−31]

Surface-tension gradients change the internal flows within drying droplets. These "Marangoni effects" produce a recirculating closed cell.[32−34] The cell transports particles away from the contact line and counteracts the buildup of a ring stain. Thermal Marangoni flows may arise on heated/cooled substrates[27,28] or through evaporative cooling.[32,35] Alternatively, solutal Marangoni flows can occur in solvent mixtures[15,23,36,37] or in the presence of surfactants.[24,38,39] However, when the droplet becomes thin, the evaporation-driven capillary flow may overcome the Marangoni flow, producing a ring stain.[15]

Received: April 1, 2014
Accepted: June 2, 2014
Published: June 2, 2014

Increasing the viscosity of the droplet during drying is an appealing way of suppressing the ring stain. However, unless the increase in the viscosity overcomes the capillary flow, a ring stain will still result. The capillary number, *Ca*, describes the ratio of viscous effects to surface tension

$$Ca = \frac{\mu v}{\sigma} \quad (1)$$

where σ is the surface tension, μ is the viscosity, and v is the fluid velocity. The order of magnitude of the velocity is $R/t_{dry} \sim 10^{-5}$ m s^{-1}, where R is the droplet radius ($\sim 10^{-5}$ m in inkjet printing) and t_{dry} is the drying time (a few seconds for water). The capillary number must approach 1 in order for viscous effects to become significant. If $Ca \geq 1$, then the droplet can deform from a spherical cap. For water, $Ca = (10^{-3}$ Pa s $\times 10^{-5}$ m s$^{-1})/10^{-1}$ N m$^{-1} \sim 10^{-7}$; a 10^7-fold increase in the viscosity during drying is required to suppress radial flow. The upper viscosity limit for inkjet printing is on the order of 10^1 mPa s at shear rates between 10^4 and 10^6 s^{-1} (depending on whether drop-on-demand or continuous inkjet systems are used), so even this extreme case requires a million-fold increase in the viscosity.

An alternative strategy for suppressing the ring stain is to exploit the elastic (rather than the viscous) properties of complex fluids. In order to overcome capillary flow and prevent particle motion, the elastic modulus of a viscoelastic fluid must exceed the capillary pressure (estimated by the Laplace pressure). We define a dimensionless number

$$\epsilon = \frac{G' r_c}{2\sigma} \quad (2)$$

as the ratio of the elastic modulus, G', to the Laplace pressure ($P = 2\sigma/r_c$) inside the droplet, where r_c is the radius of curvature of the droplet. In order to resist deformation, ϵ must be at least of the order 1. For a water-based droplet with contact angle 20° and radius 80 μm, the height, $h \sim 14$ μm, and corresponding radius of curvature, r_c, is 234 μm [$r_c = (R^2 + h^2)/2h$, where h is the droplet height]. Achieving $\epsilon = 1$ for a water droplet ($\sigma = 72.5$ mN m^{-1} at 20 °C) corresponds to an elastic modulus of $G' \sim 620$ Pa. Note that the capillary pressure decreases during drying (as the radius of curvature increases), so this is only an initial estimate for G'. A G' value of 620 Pa is more likely to be achievable than a viscosity increase on the order of 10^6. A phase transition is employed to achieve a sufficiently large elastic modulus upon printing of molten waxes or UV-cured inks.[40]

Alternatively, elasticity can be introduced into a viscous fluid by a "sol–gel" transition. A sol is a stable suspension of colloidal particles in a fluid. A gel is a complex fluid/soft solid that has elastic properties at rest but flows under shear. In a sol–gel transition, colloidal particles aggregate to form an elastic network that percolates through the fluid. A thermally activated sol–gel transition has previously been used to suppress radial convection. Printing onto a heated substrate (when the fluid gels upon heating[41,42]) and printing heated droplets onto a cool substrate (when the fluid gels upon cooling[43]) have both been demonstrated.

Radial convection is the cause of undesirable ring stains. However, if the particles do not move at all, the final deposit will be thickest at the center and thinnest at the edge (a dome). This profile results from the initially uniform particle distribution collapsing down as a 2D projection during drying. To produce a uniform particle distribution in the final deposit, a controlled amount of radial motion is required: too much radial flow and a ring stain forms; too little and a dome results. The necessary radial motion must therefore be switched off after an appropriate time.

We have used dilute suspensions of laponite (a nanoparticulate clay) to induce a sol–gel transition during evaporation at a constant temperature. As the laponite suspension becomes more concentrated inside a drying droplet, the elastic modulus of the suspension increases,[44] forming a gel capable of resisting the capillary stresses that otherwise result in particle motion. The elasticity of the gel results from the "house of cards" structure formed by the assembly of the platelike laponite particles with their negatively charged faces and positively charged edges into a network. Variation in the initial laponite concentration allows us to induce gelling after a controlled amount of evaporation. Thus, the extent of radial motion of the particles can be varied to control the final distribution of the deposit. The network breaks down when a shear force is applied, reducing the viscosity and allowing laponite suspensions that are highly viscous gels at low shear rates to be jetted in an inkjet print-head. The shear-thinning properties of laponite suspensions are also desirable for reducing satellites.[45]

As water evaporates from a droplet, the concentration of the solute (e.g., laponite) within the droplet increases, but this increase is not uniform. In the absence of convection, the concentration is highest at the air–water interface, leading to the formation of a skin if diffusion is too slow to redistribute the solute over the thickness of the droplet. Evaporation is fastest at the contact line where the drop is thinnest.[46] Consequently, the concentration of laponite increases from the apex to the contact line, and so gelation starts at the contact line and propagates inward.

In this paper, we show that the sol–gel transition in laponite suspensions can be used to suppress radial flow and form a uniform deposit. We compare the behavior of laponite suspensions with a water-soluble polymer of similar low shear viscosity (hydroxyethylcellulose, HEC) and show that laponite is more effective at suppressing ring stains.

EXPERIMENTAL SECTION

Figure 1 shows the experimental setup used to image drying picoliter droplets. Views of the side profile of the droplet and internal flows were recorded simultaneously. High-speed shadowgraph imaging was used to capture the side profiles of the droplets with a midspeed camera (Optronis CR450x3; frame rate 250 fps; exposure time 2 ms). A cold LED source was used for illumination (455 nm, Beaglehole Instruments) to prevent thermal gradients across the droplet. A

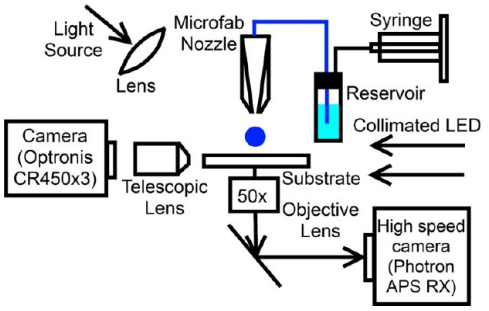

Figure 1. Cartoon of the experimental setup. The setup combines an inverted microscope with side-on shadowgraph imaging to view the internal flows and droplet profile simultaneously.

custom-written *MATLAB* routine was used to extract the evaporation rate, diameter, height, and contact angle of each droplet.

The internal flows inside drying droplets were recorded on an inverted microscope. Illumination was provided by a cold LED source (530 nm, Thorlabs), focused onto the substrate from above, at an angle (chosen to maximize image contrast). Polystyrene (PS) tracer particles were visualized as bright spots (from backscattered light) on a dark field. Images were acquired using a high-speed camera (Photron APX RS; frame rate 500 fps; exposure time 100 μs; resolution 0.4 μm × 0.4 μm) from below, through the substrate. Particle velocities were calculated using particle-tracking velocimetry code adapted from routines developed at Georgetown University.[47] The center of each particle was located and tracked through subsequent frames. Particle velocities were binned radially in increments of $0.1R$ and temporally by $0.1t_{dry}$, where R is the contact radius of the droplet and t_{dry} is the drying time. The drying time is defined as the time for the droplet volume to reach zero (determined by *MATLAB* postprocessing of the shadowgraph images and confirmed by visual inspection of the inverted microscope images). The contact radius depends on the particle position if the contact area is elliptical: R is the length of the line from the center of the droplet to the contact line, passing through the location of a given particle. The mean radial velocity (in the $x-y$ plane), $v_r(t)$, was then found for each radial bin. The tangential velocity was negligible unless the contact line depinned. Contact radii were found from fitting an ellipse to the particles at the contact line.

Picoliter droplets were ejected from a Microfab (AJ-ABP-01) drop-on-demand device, with an 80-μm orifice, controlled with a Microfab driver unit (Microfab JetDrive III Controller CT-M3-02). The waveform used to eject droplets was adjusted to emit droplets with an impact velocity of ∼1 m s^{-1} without satellites. The corresponding approximate shear rate inside the nozzle can be estimated as $u/R \sim 1$ m $s^{-1}/40 \times 10^{-6}$ m $\sim 2.5 \times 10^4$ s^{-1}, where u is the velocity of ejection and R is the radius of the nozzle orifice. Droplets dried at an ambient temperature of 21 °C and a relative humidity of 50%.

Glass coverslips were used for the deposition because of the need for a transparent substrate. The coverslips were used as received or precleaned with isopropyl alcohol to produce a more wetting substrate. Contact angles on glass substrates can vary by ±10°. Dried deposits were sputter-coated with gold (five coats at 1.2 kV, 35 mA for 30 s) before imaging by scanning electron microscopy (SEM, Philips XL30 Environmental). A white-light interferometer (Zygo NiewView 5000) provided vertical profiles of the dried deposits. The vertical noise for the interferometer was approximately ±20 nm. The vertical profiles of the deposits were azimuthally averaged in *MATLAB*.

To determine the coverage, the images of the deposits were first converted into binary form (using a threshold gray level just above the background value). The coverage was not sensitive to small variations in the threshold value. The ellipse enclosed by the contact line was sectioned into 10 concentric ellipses of equal separation. The fractional area of coverage, ϕ_n, where n indicates the ring number (1 for the innermost ring), was determined from the number of white pixels within the annulus, divided by the total number of pixels in the annulus. The total area of coverage, ϕ_t, is defined by the total number of white pixels divided by the total number of pixels within the ellipse fit to the deposit periphery. The normalized fractional area of coverage within ring n is then $\phi_{n,norm} = \phi_n/\phi_t$.

Suspensions of laponite RD (Rockwood, 30-nm-long disks, 1 nm thickness, according to the manufacturer's specification) in water (Milli-Q, 0.25 μm filter) with 0, 1, 2, and 3 wt % laponite content and containing 0.05 wt % 1-μm sterically stabilized PS spheres (PEGMA-stabilized, ζ potential of −25 to −39 mV for pH 6−9; University of Leeds, Leeds, U.K.) were prepared for particle-tracking studies. The suspension of PS spheres was made first, and the laponite was subsequently added. The laponite powder was fully hydrated, and solutions were sonicated for 15 min prior to use. No large aggregates were present in the initial formulation. Samples were made fresh on the day of jetting because of the aging properties of laponite suspensions.[48] In order to study deposits from samples with a higher solid content, laponite suspensions were prepared with 1 and 5 wt % 200-nm PS spheres. In some formulations, colloidal silica (LUDOX AS-40, Sigma-Aldrich; particle diameter ∼20 nm; ζ potential ∼ −75 mV at pH 7) was included in the laponite suspensions at concentrations up to 1 wt % as an antiaggregation agent because of the large-scale aggregates formed in deposits from laponite suspensions with PS spheres. The colloidal silica was purchased as a stable suspension and was added to the suspension of PS spheres before the laponite powder. The polymer hydroxyethylcellulose (HEC; MW 250 kg mol^{-1}, Sigma-Aldrich) was tested as a 1 wt % solution because this concentration exhibits a low shear viscosity similar to that of a 2 wt % laponite solution. Surface-tension measurements were collected for each component using a pendant drop tensiometer (First Ten Angstroms, FTA200). Note that problems with clogging did not occur for the suspensions reported in this paper.

Rheological data were collected at 293 K using an AR 2000 rheometer (TA Instruments) with a cone (2° angle) and plate geometry for laponite suspensions and HEC solutions in water, without the inclusion of PS spheres. The steady-state viscosity of each fluid was recorded over shear rates from 0.1 to 1500 s^{-1}, where the upper limit was set by the rheometer. The reported steady-state viscosities are an average of three consecutive readings within 2% of each other, and a maximum measurement time of 5 min per reading. Recovery times were investigated by applying a stepped shear rate with fast sampling. The shear rate was held at 0.1 s^{-1} for 10 min, then 1000 s^{-1} for 4 min, before returning to the low shear value (0.1 s^{-1}). The yield stress of each laponite suspension was found using oscillatory measurements with small deformations, performed by running a strain sweep (for strain values between the rheometer's lower limit of 2.88 × 10^{-3} and 0.35) at a frequency of 1 Hz. The yield stress was estimated from the product of the critical strain and the elastic modulus in the linear elastic region. The critical strain was defined as the strain at which a straight-line fit to the linear elastic and nonlinear viscoelastic regions intersected.

RESULTS AND DISCUSSION

Shear Rheology of Formulations. Figures 2 and 3 present the steady-state shear viscosity of laponite suspensions and HEC solutions over a range of shear rates. The laponite suspensions were shear-thinning when the laponite concentration exceeded about 2.5 wt %. Above 3 wt % laponite, there was no Newtonian plateau, indicating yield-stress behavior. The HEC solutions were weakly shear-thinning for HEC concentrations of 3 wt % and above. Inkjet-printed droplets experience high shear rates inside the nozzle (10^4−10^6 s^{-1} in commercial print-heads)[1] and low shear rates (10^0−10^1 s^{-1}) on the

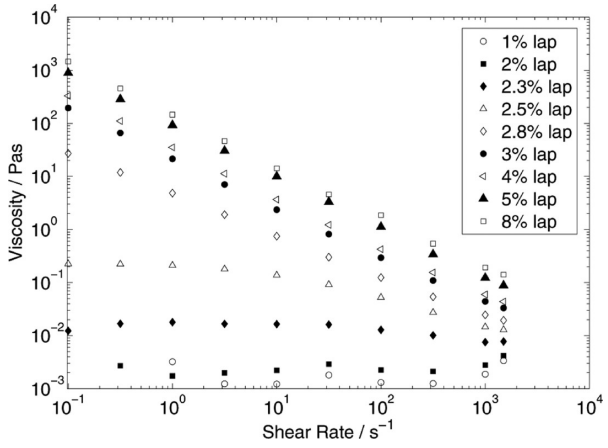

Figure 2. Steady-state shear viscosity of laponite suspensions in water as a function of the shear rate.

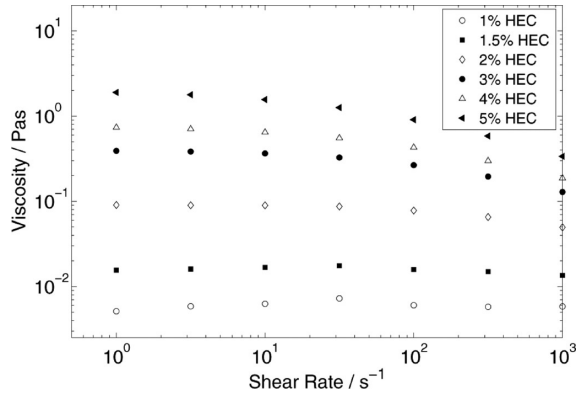

Figure 3. Steady-state shear viscosity of aqueous HEC solutions as a function of the shear rate.

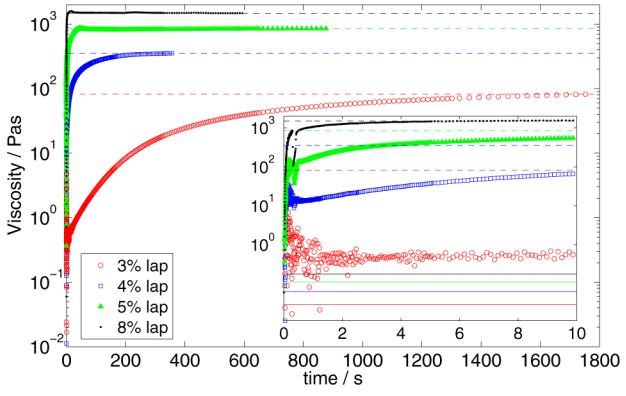

Figure 4. Recovery of the shear viscosity for laponite suspensions over a range of laponite concentrations, following a period of high shear. The inset shows the recovery of the shear viscosity over the first 10 s, encompassing the typical drying time of inkjet droplets (~5 s). Dashed horizontal lines indicate the viscosity after full recovery. Solid horizontal lines indicate the viscosity immediately following the switch from high shear rate to low shear rate.

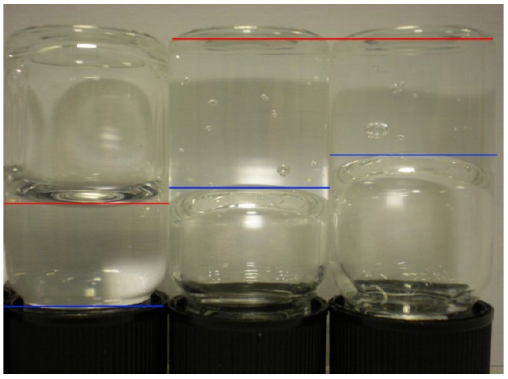

Figure 5. Inverted bottles indicating which laponite concentrations in water are sols and which are gels after wetting overnight. From left to right, the laponite concentrations are 2.8, 3, and 4 wt %. The 2.8 wt % laponite suspension is a viscous sol. The 3 and 4 wt % laponite suspensions are gels trapping bubbles. The blue horizontal lines indicate the lowest-lying part of the sample in the vial, and the red lines are the highest part.

substrate. It is therefore necessary to determine if the laponite network can recover during the lifetime of the droplet.

Figure 4 shows the recovery of the shear viscosity of laponite suspensions following a period of high shear rate. Although the applied shear was an order of magnitude lower than that in an inkjet print-head, the network was fully broken down, and so the recovery time should be the same if a shear rate of 10^4 s^{-1} was applied. For laponite concentrations $\gtrsim$3 wt %, the viscosity increased monotonically until a steady-state low-shear viscosity was attained. The recovery of the viscosity was faster for suspensions containing more laponite. For suspensions containing $\leq$5 wt % laponite, the network did not fully recover within the lifetime of a droplet (typically ~5 s). However, there was a significant viscosity increase (of order 10^2) for the 5 wt % laponite suspension over this time period. Once the laponite concentration reaches 8 wt %, the suspension fully recovers within seconds (an increase by 3 orders of magnitude in 5 s; see Figure 4). During the droplet lifetime, the increase in the laponite concentration due to evaporation will therefore facilitate total recovery of the suspension network and associated elastic properties. While the recovery of the elasticity cannot be directly measured, the recovery of the shear viscosity represents the recovery of the networked structure. If the network recovers, we can infer that the elasticity recovers.

Inverted bottle experiments (Figure 5) show a sol–gel transition between 2.8 and 3 wt % laponite. Shear rate versus shear stress curves, confirming the concentration range of the sol–gel transition, are given in the Supporting Information (Figure S1). At 3 wt % laponite, the suspension had a finite yield stress (see Table 1) and was a shear-thinning gel. The sol–gel transition gave rise to a sharp increase in the low-shear viscosity (Figure 2) and yield stress of the suspension. Note that the addition of 1 or 5 wt % 200-nm PS spheres gave a sol–gel transition between 2.5 wt % laponite (viscous sol) and 3 wt % laponite (gel) after the same time period (overnight). The

Table 1. Yield Stresses Determined by Oscillatory Measurements for Laponite Suspensions in Water at Various Laponite Concentrations

laponite/wt %	yield stress/Pa	laponite/wt %	yield stress/Pa
2.8	0.3	5.0	107
3.0	5	8.0	149
4.0	45		

Table 2. Critical Strains Determined by Oscillatory Measurements for Laponite/Silica Suspensions in Water at Various Laponite to Silica Ratios[a]

laponite/ wt %	colloidal silica/ wt %	ratio of laponite-to-silica	critical strain/%	yield stress/Pa
3.0	0.0	1:0	4.1	1.7
3.0	1.5	1:0.5	2.9	4.0
3.0	3.0	1:1	2.6	5.1
5.0	0.0	1:0	4.7	60
5.0	2.5	1:0.5	4.4	72
5.0	5.0	1:1	3.7	90

[a]Note that yield stresses for suspensions without colloidal silica differ from those in Table 1 due to different aging times.

Table 3. Surface-Tension Values, σ, for Each Component in Water at 20 °C

	component				
	water	1 wt % laponite	2 wt % laponite	1 wt % colloidal silica	1 wt % HEC
σ/mN m^{-1}	72.5	70.4	69.9	70.4	65.4

dx.doi.org/10.1021/am501966n | ACS Appl. Mater. Interfaces 2014, 6, 9572–9583

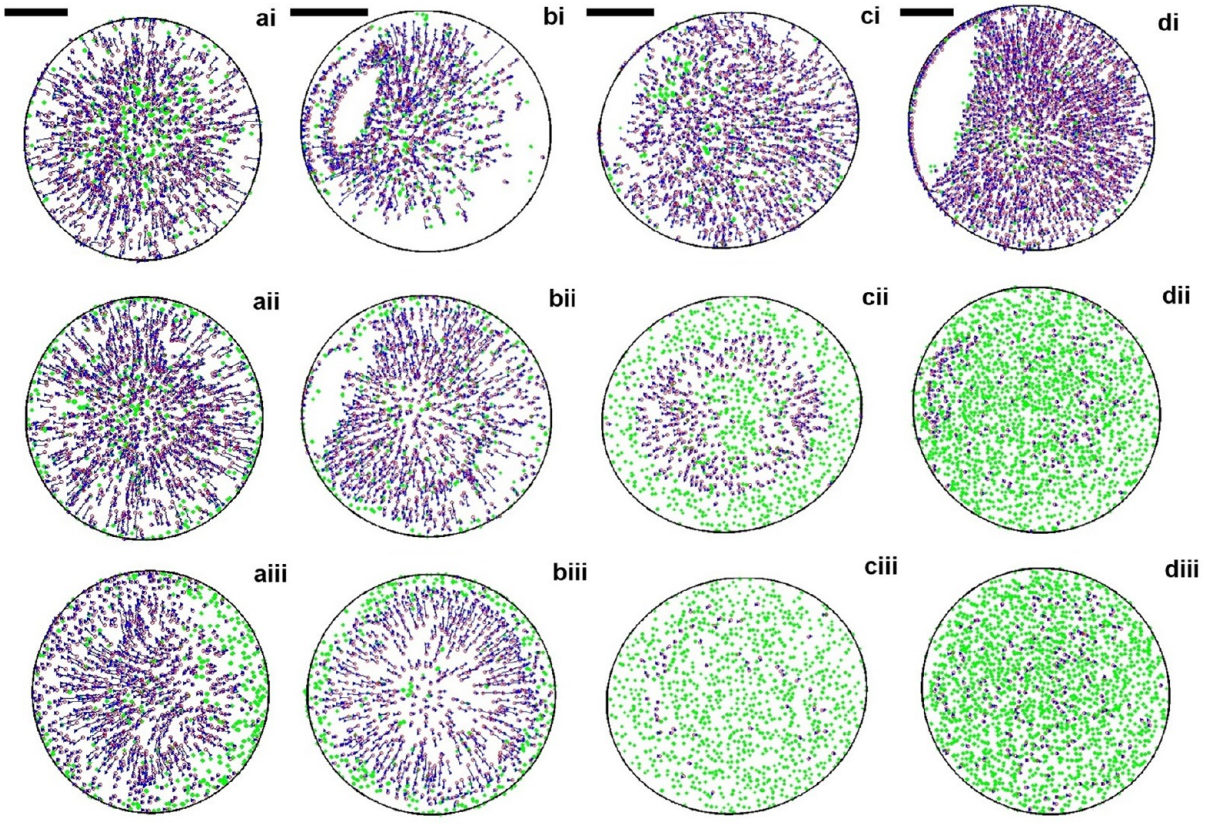

Figure 6. Particle tracks for droplets containing 0.05 wt % 1-μm PS spheres and (a) pure water (t_{dry} = 5.03 s), (b) 1 wt % HEC (t_{dry} = 5.02 s), (c) 2 wt % laponite (t_{dry} = 6.32 s), and (d) 3 wt % laponite (t_{dry} = 8.65 s). The particle tracks are shown for (i) 0.0–0.1t_{dry}, (ii) 0.4–0.5t_{dry}, and (iii) 0.7–0.8t_{dry}. Stationary particles (with movement of less than two pixels in the time interval) are indicated in green. Moving particles are indicated in blue with a red circle at the start of the track and a blue triangle at the end of the track. The black line indicates the initial contact line. Refraction of light through the droplet prevents dark-field imaging in some areas of some images, where no particles are shown. The glass slides were used as-received. The tracks are examples from single representative droplets. Scale bars are 50 μm. Example videos for a drying 2 wt % laponite suspension and a water droplet are given in the Supporting Information.

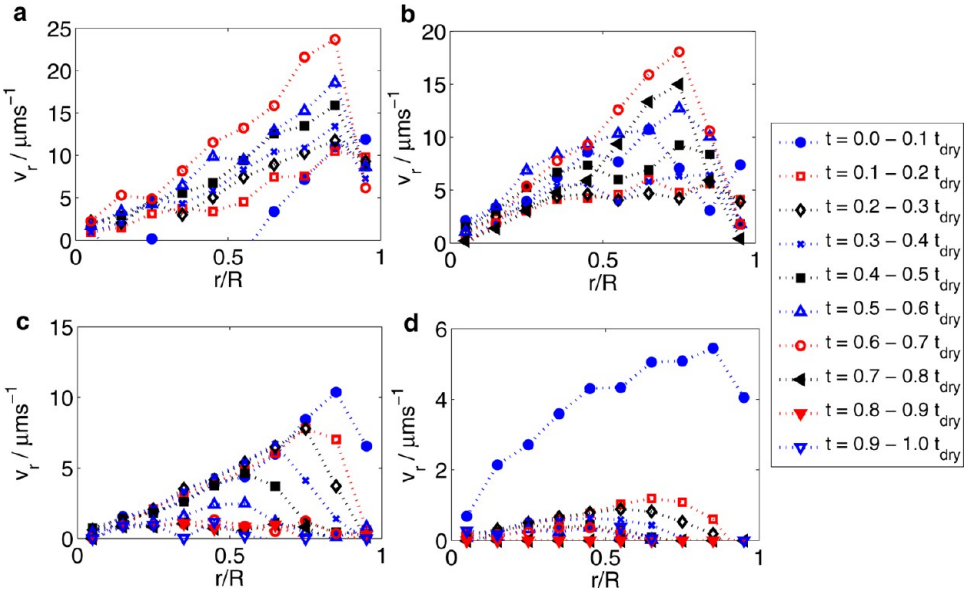

Figure 7. Mean radial velocities, v_r, over the normalized droplet radius shown for incremented temporal bins for a droplet of (a) pure water, (b) 1 wt % HEC, (c) 2 wt % laponite suspension, and (d) 3 wt % laponite suspension. Data points are plotted at the midpoint of each spatial bin. For clarity, data are shown for a single representative droplet up until the time that the contact line depins (complete data are in the Supporting Information, Figures S2 and S3).

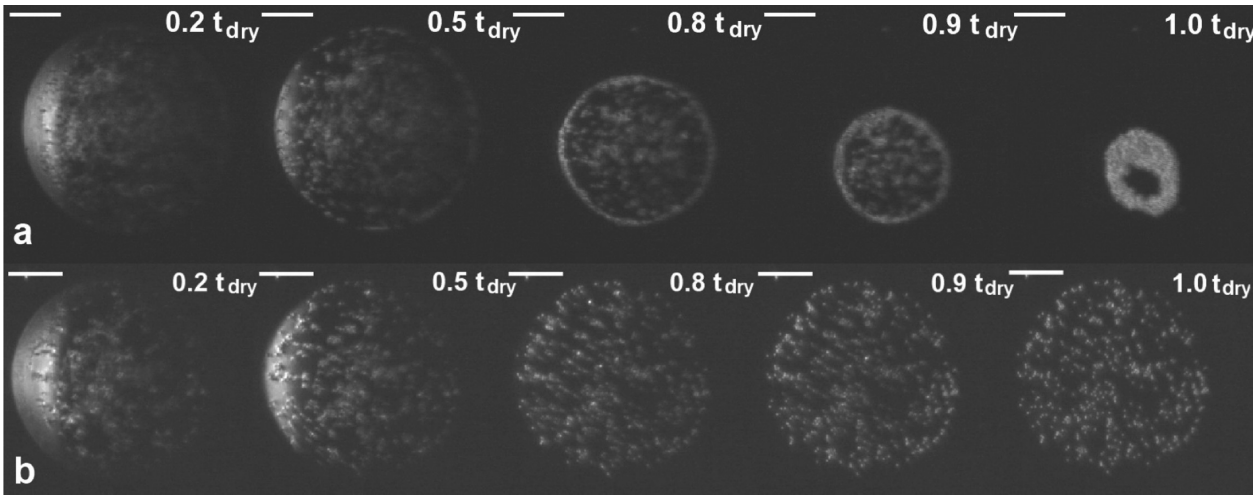

Figure 8. Inverted microscope images for (a) a droplet containing 0 wt % laponite, with 0.05 wt % 1-μm PS spheres on a glass substrate precleaned with isopropyl alcohol and (b) 2 wt % laponite. For part a, the droplet depins during drying, but for part b, the droplet stays pinned throughout drying. The scale bars are 50 μm.

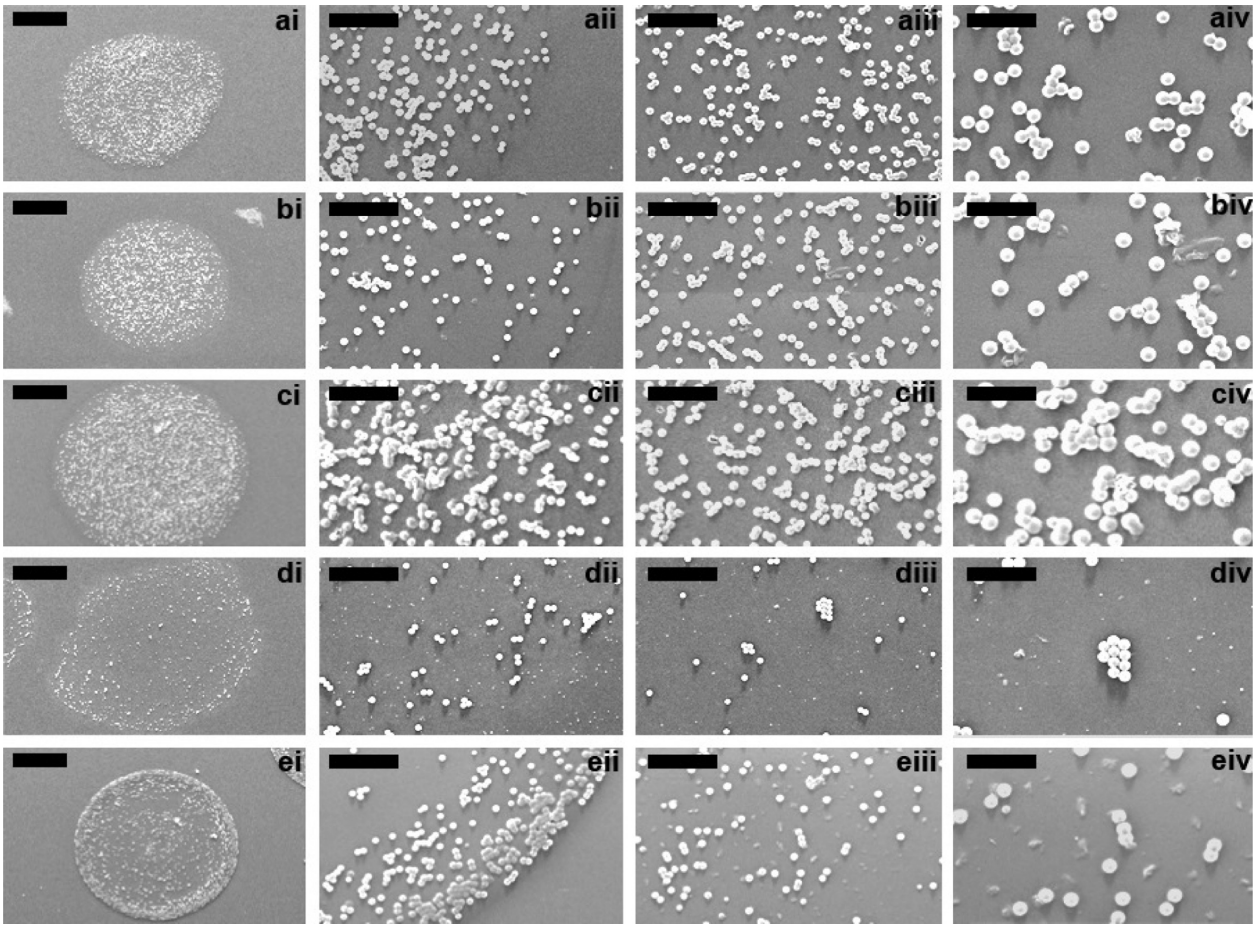

Figure 9. SEM images of deposits containing 0.05 wt % 1-μm PS spheres: (a) 1 wt % laponite; (b) 2 wt % laponite; (c) 3 wt % laponite; (d) pure water; (e) 1 wt % HEC. Images show (i) the whole droplet at a 400× zoom (scale bar 50 μm), (ii) a 2500× zoom to the contact line (scale bar 10 μm), (iii) a 2500× zoom to the interior (scale bar 10 μm), and (iv) a 5000× magnification of the interior (scale bar 5 μm). Glass substrates were used as-received.

sol−gel transition remained between 2.8 and 3 wt % laponite upon the addition of 1 wt % colloidal silica.

For our droplets (typical contact angle ∼20° and contact radius ∼80 μm), the initial capillary pressure is $p_{Ca} \sim 2\sigma/r_c \sim$ 620 Pa, where σ is the surface tension of the fluid and r_c is the radius of curvature of the droplet. The gradient in the capillary pressure that must be overcome to prevent particle motion is lower than this value. A yield stress of $\sim 10^2$ Pa is therefore required to overcome capillary flow via network elasticity (giving $\epsilon = 1$ in eq 2). Table 1 indicates that yield stresses of

dx.doi.org/10.1021/am501966n | ACS Appl. Mater. Interfaces 2014, 6, 9572−9583

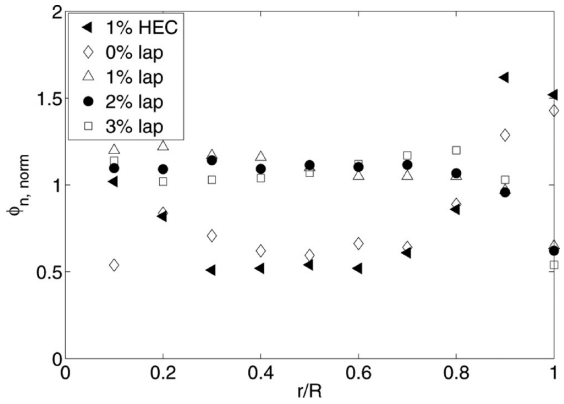

Figure 10. Radial distribution of the deposit consisting of 1-μm PS spheres at 0.05 wt % solid content. The normalized fractional area of coverage, $\phi_{n,norm}$, is plotted at the outer radial position, r, for each ring, i.e., at 0.1 for ring n = 1, encompassing r/R = 0−0.1 (where R is the deposit radius). The values are the average of at least 20 deposits.

this magnitude occur for laponite concentrations of ≥5 wt %. In comparison, a viscosity increase of a million-fold required to overcome capillary flow could not be achieved without significant solvent evaporation and so would not be achievable early enough in the drying time to prevent a ring stain. Hence, recovery of the elasticity is the important factor. We can infer from the recovery of the shear viscosity that an 8 wt % laponite suspension can fully recover the networked structure and therefore the elasticity within the lifetime of the droplet.

A comparison with HEC was performed to further confirm the recovery of the laponite suspensions during drying. For HEC, the change in the viscosity from high shear to low shear was less than an order of magnitude for any given concentration of the studied solutions. At low shear rates, the viscosity of the HEC solutions increased by 3 orders of magnitude between 1 and 5 wt %. At high shear rates, the corresponding viscosity increase was smaller ($\sim 10^2$) and comparable to the increase in the high-shear viscosity in laponite suspensions over the same concentration range. Thus, if the laponite network does not recover on the time scale of droplet drying, HEC and laponite may be expected to show similar drying behavior.

If the increase in the laponite concentration during the drying lifetime is sufficient for full network recovery, the supension will show a large viscosity increase and sol−gel transition. Once the solution becomes a gel, particle motion will be prevented, and the deposits will differ greatly from those containing HEC.

Laponite was observed to cause aggregation of PS latex particles. Colloidal silica was added to laponite suspensions to inhibit aggregation, but silica also affected the critical strain (Table 2). Increasing the ratio of silica-to-laponite decreased the critical strain, indicating a reduction in the ability of the network to maintain connectivity. The yield stress and speed of recovery of the network both increased (for a fixed laponite concentration) as the total solid concentration increased (see Supporting Information, Figure S10).

The surface tension of the laponite or silica suspensions did not differ significantly from that of water (Table 3). HEC had the largest influence, lowering the surface tension to 65.4 mN m^{-1}. The small differences in surface tension allow us to conclude that the influence of laponite and silica on the capillary pressure (and on the elastic modulus required to prevent particle motion) is small.

Evaporation and Gelation of Printed Droplets. Particle tracks (in blue) are shown in Figure 6 for an evaporating droplet of pure water, a 1 wt % polymer solution, and two concentrations of laponite suspensions (2 and 3 wt %) printed onto glass coverslips. The initial contact line is indicated by a solid black circle. For pure water (Figure 6a), the tracks are purely radial until the contact line depins near the end of the drying time (indicated by the stationary particles in green at the right-hand side of the droplet in Figure 6aiii). Figure 7a shows the mean radial velocity of the particles as a function of the radial distance from the center of the droplet for various time periods from the end of spreading until the contact line depinned (data after contact-line depinning are shown in the Supporting Information). The mean radial velocity of the particles increased throughout drying with increasing distance from the center of the droplet (apart from the rim).

The 1 wt % HEC droplet (Figure 6b) exhibited flows similar to those of the water droplet, with radial flow even at $0.8t_{dry}$, by which point the mean HEC concentration had reached 5 wt % and the low-shear viscosity had increased by more than 2 orders of magnitude. The HEC concentration was highest near the contact line, leading to a small rim of stationary particles in the final stages of drying (green particles in Figure 6biii). Figure 7b shows that the velocity profiles for 1 wt % HEC evolved similarly to pure water, with an increase in the mean radial velocity during drying. However, there was an initial decrease in the velocity at early times, potentially due to the small amount of motion in the contact line during the first time bin.

The behavior of the particles within a droplet containing laponite was very different. A droplet of 2 wt % laponite (Figure 6c) initially showed radial flow throughout the droplet, before a gelling front-propagated from the contact line toward the droplet center. Particles in the gel ceased to move (green particles in Figure 6cii), while particles in the sol continued to flow radially outward. During drying, the mean radial velocity of the particles within the droplet of 2 wt % laponite suspension decreased as the gelling front-propagated inward, reducing the velocities near the contact line at early times and closer to the center at later times (Figure 7c). Additional side images indicating the inward progression of the gelled "disk" and leaving the central sol "cap" can be found in the Supporting Information (Figure S7). Deviation of the droplet profile from a spherical cap confirms that the laponite particle network recovers quickly enough for the sol to gel within the drying time of the droplet ($t_{dry} \sim 5$ s). We note that the radial motion within the sol led to a final distribution of tracer particles (Figure 6ciii) that was highly uniform. Particle distributions in dried deposits are discussed in more detail in the following section.

The final set of particle tracks, shown in Figure 6d, are for a 3 wt % laponite suspension, which forms a shear-thinning gel. Immediately after impact and spreading there was radial flow (Figure 6di), but gelation rapidly spread throughout the entire droplet and halted particle motion (Figure 6d). The initial particle motion occurs because there is a finite recovery period after shearing of the gel in the nozzle before the laponite network reforms. We can estimate the recovery time of the gel network to be within 440 ms ($0.1t_{dry}$) from the time between droplet impact and gelation of the droplet. Figure 7d shows the radial velocity profiles for the 3 wt % laponite formulation, confirming the formation of a gel within $0.1t_{dry}$.

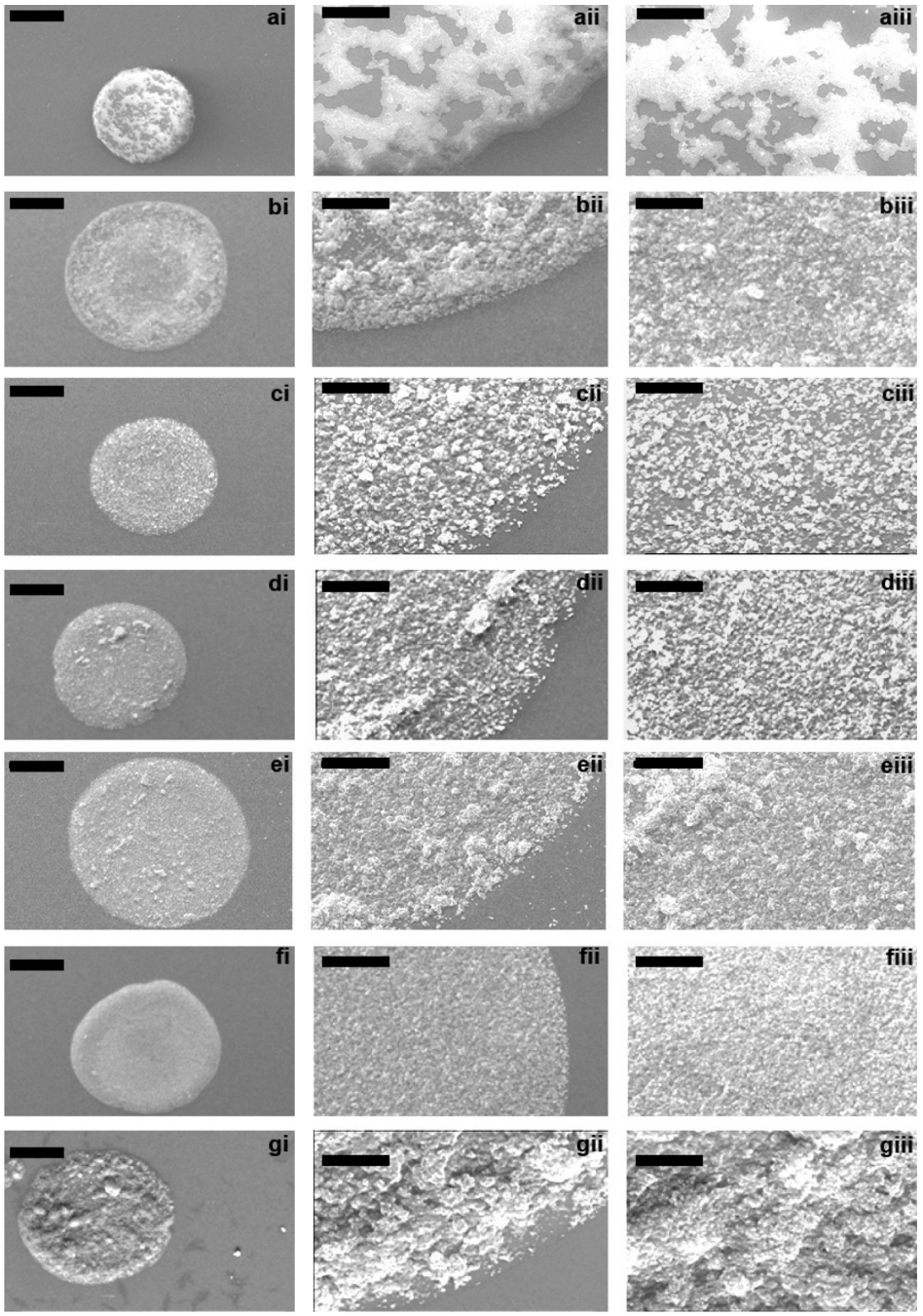

Figure 11. SEM images of deposits containing 1 wt % 200-nm PS spheres: (a) pure water; (b) 1 wt % HEC; (c) 2.8 wt % laponite; (d) 2.5 wt % laponite; (e) 2.0 wt % laponite; (f) 2 wt % laponite with 1 wt % colloidal silica; (g) 3 wt % laponite with 1 wt % colloidal silica. Segments show (i) the whole droplet (400× magnification; scale bar 50 μm), (ii) a zoom to the contact line (2500× magnification; scale bar 10 μm), and (iii) a zoom to the interior (2500× magnification; scale bar 10 μm). Substrates were as-received glass.

For droplets without laponite, the velocity of the particles increased during drying and toward the contact line. For droplets containing laponite, the velocity of the particles decreased throughout drying because particles slowed down in the gel. Plots of how the maximum velocity varies radially and temporally are given in the Supporting Information (Figures S8 and S9).

The droplets in Figure 6 were printed onto a coverslip as received from the supplier. These coverslips have varying levels of chemical contamination that increase contact-angle hysteresis, leading to pinning of the contact line. If the substrates are cleaned with isopropyl alcohol before use, pure water droplets quickly depin (Figure 8a). The receding contact line drags particles inward, leaving an irregular and unpredictable deposit shape. The gelled rim of the laponite droplet pins the contact line throughout drying (Figure 8b), resulting in a circular edge to the deposit with a radius defined by the initial spreading of the droplet on the substrate. As with the droplets printed on as-received glass, the width of the gelled ring grew as evaporation progressed with the freely flowing suspension restricted to a region of decreasing radius around the center of the droplet.

In this section, we have established that laponite controls the amount of radial flow in evaporating droplets. It is the radial flow that is responsible for forming ring-stain deposits in drying

dx.doi.org/10.1021/am501966n | ACS Appl. Mater. Interfaces 2014, 6, 9572−9583

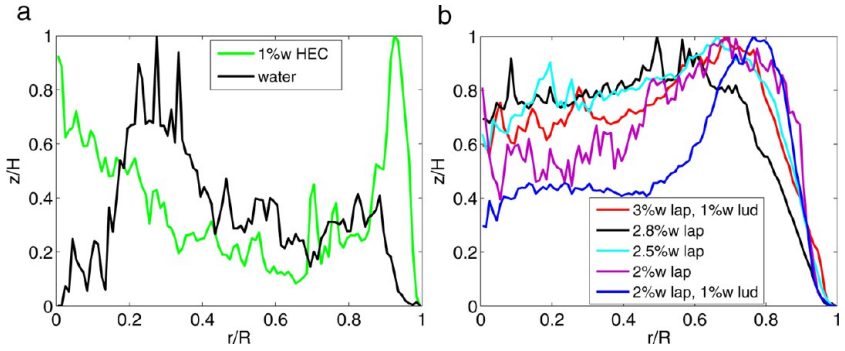

Figure 12. Azimuthally averaged height profiles taken on a white-light interferometer for deposits of (a) water droplets containing 1 wt % 200-nm PS spheres with and without HEC and (b) various concentrations of laponite and colloidal silica. The deposit height, z, at a radius, r, from the deposit center is normalized by the maximum height of the deposit, H. R is the deposit radius.

droplets. However, in order to form a uniform deposit rather than a dome, some radial motion is necessary. The combination of the concentration of the laponite during drying and a fast recovery time of the networked structure is essential to control the extent of radial flow. In the following section, we examine dried deposits to determine if, by using laponite to reduce the radial flow, we can control the particle distribution and eliminate ring stains.

Distribution of Tracers in a Dry Deposit. Figure 9 shows scanning electron micrographs of the dried deposits from various formulations containing 0.05 wt % 1-μm tracer PS spheres. From these micrographs, we calculated the fraction of the substrate covered by PS spheres as a function of the radial distance from the center of the deposit. Figure 10 plots these distributions, normalized to the average density. The laponite suspensions provided a more uniform distribution of tracer particles than either water or 1 wt % HEC, both of which show an increase in the particle density toward the edge of the deposit (a ring stain). The 1 wt % HEC solution also shows a buildup of particles at the center of the deposit. In laponite suspensions containing only a trace amount of solids, the laponite concentration made little difference to the area covered by the deposit. The 1, 2, and 3 wt % laponite suspensions produced a uniform density of particles across most of the deposit, except near the contact line, where the particle density decreased (Figure 9a–c).

Close inspection of the high-resolution images (Figure 9, column iv) shows that the diameter of the PS spheres deposited from 3 wt % laponite appears to be nearly double that in pure water. The explanation is that during drying the nanoparticles of laponite coat the PS sphere. The change in the size of the spheres is less evident for the lower laponite concentrations, but the outlines of the spheres are less sharp than those for the water droplet (Figure 9d) and the spheres blend into each other where they are in contact, owing to the laponite coating between the spheres. The HEC deposit shows a polymer coating on the spheres near the contact line where the HEC ring stain forms (Figure 9eii).

Deposits with a High Solid Content. In the previous section, we demonstrated that control of radial flow in laponite suspensions can lead to uniform coverage of the tracer particles in a dried deposit. We now investigate whether the same uniformity can be achieved in formulations with a higher fraction of suspended solids, for which we chose 200-nm PS spheres at concentrations of 1 and 5 wt %.

Figure 11 shows SEM micrographs of droplet deposits containing 1 wt % 200-nm PS spheres. The droplet of water depinned during drying and produced a highly nonuniform distribution with a holey structure consisting of patches of covered and bare substrate (Figure 11a). The interferometric profile (Figure 12a) confirmed the nonuniform thickness. As expected, because of the depinning, there was no significant ring structure at the contact line. For a droplet containing 1 wt % HEC, the deposit had a thin ring at the edge and a nonuniform radial profile (Figure 11b). Interferometry revealed that the deposit had a raised central region as well as a ring at the contact line (Figure 12a). Droplets containing laponite (Figure 11c–e) produced more uniform radial particle distributions with fewer patches. The interferometry profiles show that laponite concentrations of 2.8 and 2.5 wt % formed fairly flat deposits (Figure 12b), while the 2 wt % suspension had a dip at the center, indicating that gelation took place too late in the drying process to suppress ring formation completely.

While laponite generated spatially more uniform deposits, it had the negative effect of promoting aggregation of the PS colloids during the drying process, as shown by the many large aggregates in Figure 11c–e. A possible explanation is that the laponite plates with positively charged edges can bridge between negatively charged PS spheres. These large aggregates give rise to an undesirable rough texture in the deposits. In order to suppress aggregation of the PS spheres induced by the laponite, we added 1 wt % colloidal silica to the 2 wt % laponite solution. The silica reduced the number of large aggregates and produced a much smoother surface texture (compare parts e and f of Figure 11). The suspensions containing colloidal silica were less effective at suppressing the ring stain. It is possible that the lower critical strain in suspensions containing silica (Table 2) reduces the ability of loose aggregates to remain connected under the gentle shear within the drying droplet. Without connectivity throughout the suspension, the elasticity cannot recover. Consequently, particles move outward with radial flow and build up a ring, similar to pinned droplets without laponite (Figure 12b). To increase the critical strain, we increased the laponite concentration to 3 wt % at fixed silica concentration and obtained a fairly uniform pancake deposit (Figure 12b). However, aggregates formed once again (Figure 11g), indicating a trade-off between ring suppression and aggregate formation dependent on the laponite-to-silica ratio, which would have to be optimized in an ink formulation.

SEM micrographs of dry deposits formed from suspensions of 5 wt % PS spheres are shown in Figure 13, with the azimuthally averaged height profiles shown in Figure 14. For both pure water and 1 wt % HEC, the footprint of the drop was

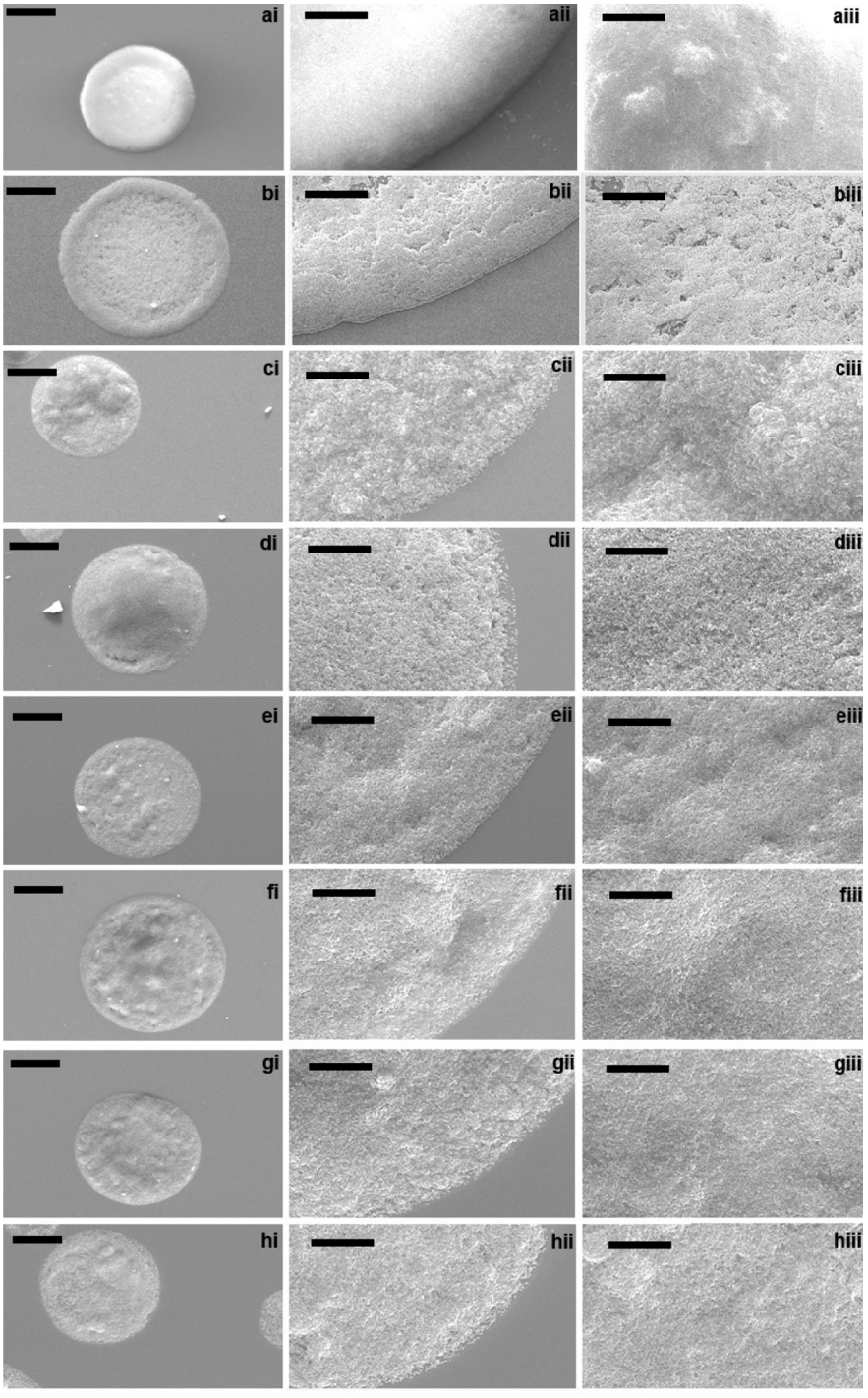

Figure 13. SEM images of deposits containing 5 wt % 200-nm PS spheres: (a) pure water; (b) 1 wt % HEC; (c) 2 wt % laponite; (d) 1 wt % laponite; (e) 0.8 wt % laponite; (f) 2 wt % laponite and 1 wt % colloidal silica; (g) 1 wt % laponite and 1 wt % colloidal silica; (h) 0.8 wt % laponite and 1 wt % colloidal silica. Segments show (i) the whole droplet (400× magnification; scale bar 50 μm), (ii) a zoom to the contact line (2500× magnification; scale bar 10 μm), and (iii) a zoom to the interior (2500× magnification; scale bar 10 μm). Substrates were as-received glass.

completely covered by PS spheres, but there was a pronounced ring stain (Figure 13a,b). Upon the addition of 2 or 1 wt % laponite, the deposit had a domed morphology with large aggregates (Figure 13c) or cracking near the periphery (Figure 13d). The sol−gel transition occurred too quickly to allow sufficient radial motion of the PS particles. The vertical profile of the deposit was then thicker where the droplet was highest. The presence of a high concentration of PS nanospheres appears to reduce the amount of laponite needed to form a gel. Reducing the laponite concentration to 0.8 wt % delayed gelation and yielded a fairly flat pancake. However, the presence of large aggregates resulted in uneven deposition and a rough surface texture (Figure 13e). Further addition of 1 wt % colloidal silica reduced the peripheral cracking in the 1 wt % laponite droplet (Figure 13g), and the number of aggregates in the 0.8 wt % laponite deposit (Figure 13h), although aggregates still remained in the 2 wt % laponite droplet (Figure 13f).

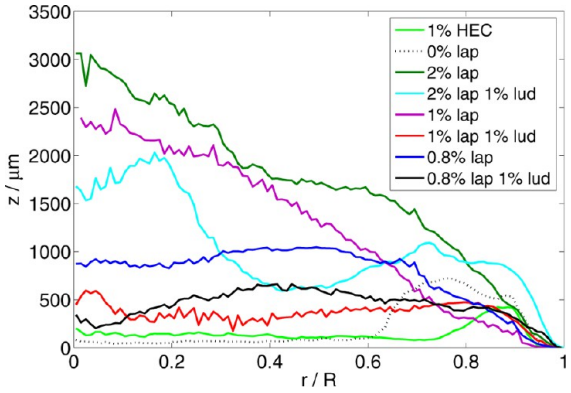

Figure 14. Azimuthally averaged height profiles taken on a white-light interferometer, for deposits of water droplets containing 5 wt % 200-nm PS spheres and either HEC or various concentrations of laponite and colloidal silica. The deposit height, z, at a radius, r, from the deposit center is shown, where the radius is normalized by the maximum radius of the deposit, R.

The networking properties of the laponite/colloidal silica mixtures will depend on the ratio of laponite to colloidal silica, and the gelation point also depends on the total solid volume fraction (including the PS spheres). We have not attempted to optimize this formulation, but the flatness and uniformity of the profile formed from the 1 wt % laponite droplet containing 1 wt % colloidal silica is already very encouraging.

CONCLUSIONS

Formulation of colloidal suspensions for inkjet printing is a complex problem that involves balancing the competing requirements of the fluid. The formulation must be stable during storage and jettable from an inkjet print-head, and it must dry on the substrate to give the desired morphology of the deposit. This paper has focused on the last of these problems, and specifically on counteracting the "ring stains" that arise from convective flow toward a pinned contact line. The capillary numbers in inkjet-printed droplets are exceedingly low ($\sim 10^{-6}$), and an increase in the viscosity alone during drying was inadequate to prevent the formation of a ring stain.

Fluids that undergo a sol−gel transition as the concentration of the structuring agent increases generate elasticity in the fluid. If the yield stress of the fluid exceeds the capillary pressure, then the convective flow to the contact line (which generates the ring stain) may be stemmed. We have shown that an evaporation-driven sol−gel transition in laponite suspensions can be used to control the morphology of a deposit for a model colloidal suspension (comprising sterically stabilized latex spheres). The enhanced evaporation rate near the contact line causes the droplet to gel first at its rim, with the gelled region progressing inward to the center of the droplet. By controlling the laponite concentration and, hence, the timing of the gelling, we can dictate the amount of radial flow required to generate a uniform deposit: too little radial flow and a domed structure forms, but too much and a ring stain is produced.

The non-Newtonian rheology of the fluid is an essential component in the formulation. To be stable during storage, we require the initial suspension to have a yield stress, which arises from the network formed between the nanoparticulate plates of the clay. Under the high shear of the inkjet nozzle, the network breaks down and the fluid shear thins such that its Ohnesorge number is within the compatible range of the inkjet print-head. The finite time taken to rebuild the laponite network is also important: if the network rebuilds too quickly, the droplet will gel before it begins to dry and a domed deposit will result; if it is too slow, the droplet will gel too late in the drying process, after the ring stain has begun to form. The recovery time of the network decreases as the laponite concentration increases, and it is the balance of the increasing concentration of laponite during drying and the corresponding decrease in the recovery time that provides the necessary control over the gelling of the droplet.

The presence of laponite in the formulation had a further benefit of pinning the contact line throughout drying and enabling the formation of a circular deposit of well-defined diameter.

The addition of a new component to a formulation can have undesirable side effects. In this case, we found that laponite was prone to inducing aggregation of the latex spheres. Colloidal silica was found to be a suitable additive for reducing large-scale aggregation and providing a smoother surface texture to deposits. However, colloidal silica reduced the critical strain of the laponite suspensions, which favored the formation of ring staining. A careful balance of the silica-to-laponite ratio was needed to ensure a flat deposit profile with reduced aggregation and a smooth surface texture, while maintaining suitable rheological properties for storage and jetting.

ASSOCIATED CONTENT

Supporting Information

Additional figures and videos. This material is available free of charge via the Internet at http://pubs.acs.org.

AUTHOR INFORMATION

Corresponding Author

*E-mail: c.d.bain@durham.ac.uk. Phone: +44 (0)191 3342138. Fax: +44 (0)191 334 2051.

Notes

The authors declare no competing financial interest.

ACKNOWLEDGMENTS

The authors thank H. N. Yow and S. Biggs (Leeds University, Leeds, U.K.) for providing the PS spheres and ζ potentials. This work was supported financially by EPSRC under Grant EP/H018913/1.

REFERENCES

(1) Hutchings, I. M.; Martin, G. D. *Inkjet Technology for Digital Fabrication*, 1st ed.; Wiley-Blackwell: Hoboken, NJ, 2012.
(2) Sobac, B.; Brutin, D. Triple-Line Behavior and Wettability Controlled by Nanocoated Substrates: Influence on Sessile Drop Evaporation. *Langmuir* **2011**, *27*, 14999−15007.
(3) Jokinen, V.; Sainiemi, L.; Franssila, S. Controlled Lateral Spreading and Pinning of Oil Droplets Based on Topography and Chemical Patterning. *Langmuir* **2011**, *27*, 7314−7320.
(4) Léopoldès, J.; Dupuis, A.; Bucknall, D. G.; Yeomans, J. M. Jetting Micron-Scale Droplets onto Chemically Heterogeneous Surfaces. *Langmuir* **2003**, *19*, 9818−9822.
(5) Larsen, S. T.; Taboryski, R. A Cassie-Like Law Using Triple Phase Boundary Line Fractions for Faceted Droplets on Chemically Heterogeneous Surfaces. *Langmuir* **2009**, *25*, 1282−1284.
(6) Deegan, R. D. Pattern formation in drying drops. *Phys. Rev. E* **2000**, *61*, 475−485.
(7) Maheshwari, S.; Zhang, L.; Zhu, Y.; Chang, H.-C. Coupling Between Precipitation and Contact-Line Dynamics: Multiring Stains and Stick-Slip Motion. *Phys. Rev. Lett.* **2008**, *100*, 044503.

(8) Sangani, A. S.; Lu, C.; Su, K.; Schwarz, J. A. Capillary force on particles near a drop edge resting on a substrate and a criterion for contact line pinning. *Phys. Rev. E* **2009**, *80*, 011603.
(9) Deegan, R. D.; Bakajin, O.; Dupont, T. F.; Huber, G.; Nagel, S. R.; Witten, T. A. Contact line deposits in an evaporating drop. *Phys. Rev. E* **2000**, *62*, 756−765.
(10) Faers, M. A.; Pontzen, R. Factors influencing the association between active ingredient and adjuvant in the leaf deposit of adjuvant-containing suspoemulsion formulations. *Pest Manage. Sci.* **2008**, *64*, 820−833.
(11) Shen, X.; Ho, C.-M.; Wong, T.-S Minimal Size of Coffee Ring Structure. *J. Phys. Chem. B* **2010**, *114*, 5269−5274.
(12) Dou, R.; Wang, T.; Guo, Y.; Derby, B. Ink-Jet Printing of Zirconia: Coffee Staining and Line Stability. *J. Am. Ceram. Soc.* **2011**, *94*, 3787−3792.
(13) Friederich, A.; Binder, J. R.; Bauer, W. Rheological Control of the Coffee Stain Effect for Inkjet Printing of Ceramics. *J. Am. Ceram. Soc.* **2013**, *1*, 1−7.
(14) Deegan, R. D.; Bakajin, O.; Dupont, T. F.; Huber, G.; Nagel, S. R.; Witten, T. A. Capillary flow as the cause of ring stains from dried liquid drops. *Nature* **1997**, *389*, 827−829.
(15) Talbot, E. L.; Berson, A.; Bain, C. D. Drying and Deposition of Picolitre Droplets of Colloidal Suspensions in Binary Solvent Mixtures. *NIP28: 28th International Conference on Digital Printing Technologies and Digital Fabrication*, Quebec City, Canada, Sept 9−13, 2012; The Society for Imaging Science and Technology: Springfield, VA, 2012; pp 420−423.
(16) Talbot, E. L.; Berson, A.; Bain, C. D. Internal Flows and Particle Transport Inside Picoliter Droplets of Binary Solvent Mixtures. *NIP29: 29th International Conference on Digital Printing Technologies and Digital Fabrication*, Sept 29−Oct 3, 2013; The Society for Imaging Science and Technology: Springfield, VA, 2013; Vol. *28*, pp 307−312.
(17) Vaseem, M.; Lee, K. M.; Hong, A.-R.; Hahn, Y.-B. Inkjet Printed Fractal-Connected Electrodes with Silver Nanoparticle Ink. *ACS Appl. Mater. Interfaces* **2012**, *4*, 3300−3307.
(18) Fribourg-Blanc, E.; Dang, D. M. T.; Dang, C. M. Characterization of silver nanoparticle based inkjet printed lines. *Microsyst. Technol.* **2013**, *19*, 1961−1971.
(19) Wang, B.-Y.; Yoo, T.-H.; Song, Y.-W.; Lim, D.-S.; Oh, Y.-J. Cu Ion Ink for a Flexible Substrate and Highly Conductive Patterning by Intensive Pulsed Light Sintering. *ACS Appl. Mater. Interfaces* **2013**, *5*, 4113−4119.
(20) Roth, E. A.; Xu, T.; Das, M.; Gregory, C.; Hickman, J. J.; Boland, T. Inkjet printing for high-throughput cell patterning. *Biomaterials* **2004**, *25*, 3707−3715.
(21) Ko, S. H.; Pan, H.; Grigoropoulos, C. P.; Luscombe, C. K.; Fréchet, J. M. J.; Poulikakos, D. All-inkjet-printed flexible electronics fabrication on a polymer substrate by low-temperature high-resolution selective laser sintering of metal nanoparticles. *Nanotechnology* **2007**, *18*, 1−8.
(22) Schirmer, N. C.; Ströhle, S.; Tiwari, M. K.; Poulikakos, D. On the Principles of Printing Sub-micrometer 3D Structures from Dielectric-Liquid-Based Colloids. *Adv. Funct. Mater.* **2011**, *21*, 388−395.
(23) Park, J.; Moon, J. Control of Colloidal Particle Deposit Patterns within Picoliter Droplets Ejected by Ink-Jet Printing. *Langmuir* **2006**, *22*, 3506−3513.
(24) Kajiya, T.; Kobayashi, W.; Okuzono, T.; Doi, M. Controlling the Drying and Film Formation Processes of Polymer Solution Droplets with Addition of Small Amount of Surfactants. *J. Phys. Chem. B* **2009**, *113*, 15460−15466.
(25) Kim, D.; Jeong, Y.; Koo, C. Y.; Song, K.; Moon, J. Thin Film Transistors with Ink-Jet Printed Amorphous Oxide Semiconductors. *Jpn. J. Appl. Phys.* **2010**, *49*, 05EB06.
(26) Cui, L.; Zhang, J.; Zhang, X.; Huang, L.; Wang, Z.; Li, Y.; Gao, H.; Zhu, S.; Wang, T.; Yang, B. Suppression of the Coffee Ring Effect by Hydrosoluble Polymer Additives. *ACS Appl. Mater. Interfaces* **2012**, *47*, 2775−2780.
(27) Soltman, D.; Subramanian, V. Inkjet-Printed Line Morphologies and Temperature Control of the Coffee Ring Effect. *Langmuir* **2008**, *24*, 2224−2231.
(28) Hendarto, E.; Gianchandani, Y. B. Size sorting of floating spheres based on Marangoni forces in evaporating droplets. *J. Micromech. Microeng.* **2013**, *23*, 1−7.
(29) Kim, S. J.; Kang, K. H.; Lee, J.-G.; Kang, I. S.; Yoon, B. J. Control of Particle-Deposition Pattern in a Sessile Droplet by Using Radial Electroosmotic Flow. *Anal. Chem.* **2006**, *78*, 5192−5197.
(30) Ko, S. H.; Lee, H.; Kang, K. H. Hydrodynamic Flows in Electrowetting. *Langmuir* **2008**, *24*, 1094−1101.
(31) Eral, H. B.; Augustine, D. M.; Duits, M. H. G.; Mugele, F. Suppressing the coffee stain effect: how to control colloidal self-assembly in evaporating drops using electrowetting. *Soft Matter* **2011**, *7*, 4954−4958.
(32) Hu, H.; Larson, R. G. Analysis of the Effects of Marangoni Stresses on the Microflow in an Evaporating Sessile Droplet. *Langmuir* **2005**, *21*, 3963−3971.
(33) Hu, H.; Larson, R. G. Marangoni Effect Reverses Coffee-Ring Depositions. *J. Phys. Chem. B* **2006**, *110*, 7090−7094.
(34) Hamamoto, Y.; Christy, J. R. E.; Sefiane, K. The Flow Characteristics of an Evaporating Ethanol−Water Mixture Droplet on a Glass Substrate. *J. Therm. Sci. Technol.* **2012**, *7*, 425−436.
(35) Ristenpart, W. D.; Kim, P. G.; Domingues, C.; Wan, J.; Stone, H. A. Influence of Substrate Conductivity on Circulation Reversal in Evaporating Drops. *Phys. Rev. Lett.* **2007**, *99*, 234502.
(36) Lim, J. A.; Lee, W. H.; Lee, H. S.; Lee, J. H.; Park, Y. D.; Cho, K. Self-Organization of Ink-jet-Printed Triisopropylsilylethynyl Pentacene via Evaporation-Induced Flows in a Drying Droplet. *Adv. Funct. Mater.* **2008**, *18*, 229−234.
(37) de Gans, B.-J.; Schubert, U. S. Inkjet Printing of Well-Defined Polymer Dots and Arrays. *Langmuir* **2004**, *20*, 7789−7793.
(38) Truskett, V. N.; Stebe, K. J. Influence of Surfactants on an Evaporating Drop: Fluorescence Images and Particle Deposition Patterns. *Langmuir* **2003**, *19*, 8271−8279.
(39) Still, T.; Yunker, P. J.; Yodh, A. G. Surfactant-Induced Marangoni Eddies Alter the Coffee-Rings of Evaporating Colloidal Drops. *Langmuir* **2012**, *28*, 4984−4988.
(40) Cox, W. R.; Chen, T.; Guan, C.; Hayes, D. J.; Hoenigm, R. E.; Teipen, B. T.; MacFarlane, D. Micro-jet Printing of Refractive Microlenses. *Proceedings OSA Diffractive Optics and Micro-Optics Topical Meeting*, Kailua-Kona, Hawaii, June 1998; Optical Society of America: Washington, DC, 1998.
(41) van den Berg, A. M. J.; de Laat, A. W. M.; Smith, P. J.; Perelaera, J.; Schubert, U. S. Geometric control of inkjet printed features using a gelating polymer. *J. Mater. Chem.* **2007**, *17*, 677−683.
(42) Sun, K.; Raghavan, S. R. Thermogelling Aqueous Fluids Containing Low Concentrations of Pluronic F127 and Laponite Nanoparticles. *Langmuir* **2010**, *26*, 8015−8020.
(43) Alfred, D. R. (Dataproducts Corp.). Formulation for depositing a material on a substrate using ink jet printing. European Patent 0329026B1, 1993.
(44) Mourchid, A.; Delville, A.; Levitz, P. Sol−Gel Transition of Colloidal Suspensions of Anisotropic Particles of Laponite. *Faraday Discuss.* **1995**, *101*, 275−285.
(45) Hoath, S. D.; Jung, S.; Hsiao, W.-K.; Hutchings, I. M. How PEDOT:PSS solutions produce satellite-free inkjets. *Org. Electron.* **2012**, *13*, 3259−3262.
(46) Hu, H.; Larson, R. G. Evaporation of a Sessile Droplet on a Substrate. *J. Phys. Chem. B* **2002**, *106*, 1334−1344.
(47) www.http://physics.georgetown.edu/matlab/tutorial.html. Viewed 15/07/2013.
(48) Joshi, Y. M.; Ranjith, G.; Reddy, K.; Kulkarni, A. L.; Kumar, N.; Chhabra, R. P. Rheological behaviour of aqueous suspensions of laponite: new insights into the ageing phenomena. *Proc. R. Soc. A* **2008**, *464*, 469−489.